biology letters
Biomechanics

Biol. Lett. (2010) **6**, 394–397
doi:10.1098/rsbl.2009.0806
Published online 3 February 2010

Vortex interactions with flapping wings and fins can be unpredictable

David Lentink[1,*], GertJan F. Van Heijst[2], Florian T. Muijres[1] and Johan L. Van Leeuwen[1]

[1]*Experimental Zoology Group, Wageningen University, 6709 PG Wageningen, The Netherlands*
[2]*Department of Physics, Eindhoven University of Technology, 5600 MB Eindhoven, The Netherlands*
**Author for correspondence (david.lentink@wur.nl).*

As they fly or swim, many animals generate a wake of vortices with their flapping fins and wings that reveals the dynamics of their locomotion. Previous studies have shown that the dynamic interaction of vortices in the wake with fins and wings can increase propulsive force. Here, we explore whether the dynamics of the vortex interactions could affect the predictability of propulsive forces. We studied the dynamics of the interactions between a symmetrically and periodically pitching and heaving foil and the vortices in its wake, in a soap-film tunnel. The phase-locked movie sequences reveal that abundant chaotic vortex-wake interactions occur at high Strouhal numbers. These high numbers are representative for the fins and wings of near-hovering animals. The chaotic wake limits the forecast horizon of the corresponding force and moment integrals. By contrast, we find periodic vortex wakes with an unlimited forecast horizon for the lower Strouhal numbers (0.2–0.4) at which many animals cruise. These findings suggest that swimming and flying animals could control the predictability of vortex-wake interactions, and the corresponding propulsive forces with their fins and wings.

Keywords: swimming; flight; flapping; chaos; vortex; interaction

1. INTRODUCTION

Many swimming and flying animals create large vortices with their fins and wings. These vortices are shed, and together they form the 'footprint' of the animal in the fluid: the wake. In the wake, vortices arrange in shapes and patterns that not only reflect the motion of animals, but also the dynamics of vortex–vortex and vortex–animal interactions. Two well-known examples of intense vortex–vortex interactions are vortex merging (Cerretelli & Williamson 2003) and stripping (Legras & Dritschel 1993). In some cases, vortex–animal interactions are beneficial to an animal's locomotory performance. Insects, for example, can recapture their vortex wake and thus generate extra lift (Dickinson *et al.* 1999) while some fishes tune their body wave to exploit vortices in the wake of obstacles in running water (Liao *et al.* 2003). The dynamics of wake vortices might, however, not always be as easy to tune into.

Vortex wakes of animals are typically envisioned as a periodic row of alternating vortices. This is contradicted by several computational fluid dynamic studies of two-dimensional pitching and heaving (flapping) foils that model swimming and flight (Lentink & Gerritsma 2003; Lewin & Haj-Hariri 2003; Alben & Shelley 2005; Blondeaux *et al.* 2005; Iima 2007), which report the existence of some aperiodic and chaotic vortex wakes. These chaotic vortex wakes mediate chaotic fluid forces on foils, with a corresponding strange attractor in the phase plot of fluid lift and thrust, and are accompanied by a broad frequency spectrum and sensitivity to initial conditions (Lentink & Gerritsma 2003). Further studies in which the foil propels itself through the fluid show that these chaotic forces result in chaotic body motion of which the extent is determined by the relative inertia of the foil (Alben & Shelley 2005; Iima 2007). If animals actually need to cope with chaotic vortex interactions and forces, it might well constrain their neural control of body motion. There exists, however, no experimental confirmation of chaotic vortex-wake interactions generated by pitching and heaving foils. Further, it is unknown to what extent vortex interactions are chaotic in the parametric domain of pitching and heaving foils representative for animal fins and wings. Here, we study these vortex interactions with a two-dimensional flapping foil in a soap tunnel for a wide range of kinematics representative for slender animal wings and fins (e.g. Lentink & Dickinson 2009).

2. MATERIAL AND METHODS

We refer to Muijres & Lentink (2007) for a detailed description of the set-up and method, and to Lentink *et al.* (2008) for theory.

(a) *Flapping foil in a soap tunnel*

Our foil pitches and heaves periodically and symmetrically, with 90° out of phase sinusoidal kinematics, in a nearly horizontal, gravity driven, soap-film tunnel that flows at approximately $0.25\ \mathrm{m\,s^{-1}}$. We chose symmetric and periodic foil kinematics to ensure that measured asymmetric and aperiodic vortex-wake interactions can be linked explicitly to vortex dynamics. The foil is 5 per cent thick and flaps at 4–25 Hz.

(b) *Flapping parameters*

The flapping foil generates thrust when the effective angle of attack is larger than zero: $\alpha_{\mathrm{eff}} = \alpha_{\mathrm{ind}} - \alpha_0 > 0°$ (figure 1), which occurs when the angle of attack amplitude induced by the foil's flapping motion $\alpha_{\mathrm{ind}} = \arctan\,(2\pi \times A^*/\lambda^*)$ is larger than the pitch amplitude α_0 ($A^* = A/c$, dimensionless heave amplitude; $\lambda^* = U_\infty/fc$, dimensionless heave length; A, heave amplitude; c, chord length; U_∞, free stream velocity; f, flap frequency). The combinations of (A^*, λ^*, α_0) studied here are all combinations of ($A^* = 0, 1, \ldots, 4$; $\lambda^* = 3, 5, \ldots, 13$; $\alpha_0 = 0°, 15°, \ldots, 90°$) for which $\alpha_{\mathrm{eff}} \geq 0°$. The average Reynolds number Re of the foil is $Re \approx Re_\infty \times \sqrt{1 + (4A^*/\lambda^*)^2}$, in which $Re_\infty = U_\infty \times c/\nu \approx 1000$ is the free stream Reynolds number (Re is of order 1000; soap-film kinematic viscosity $\nu \approx 1 \times 10^{-6}\ \mathrm{m^2\,s^{-1}}$ (Martin & Wu 1995)).

(c) *Flow visualization and image analysis*

We filmed the vortex wake of the foil time (500 Hz) and space resolved (1024 × 1280 pixels) as a function of (A^*, λ^*, α_0), and phase-locked over 99 periods; at stroke reversal and midstroke. We obtained interference fringes by illuminating the soap film with a monochromatic SOX lamp (Rutgers *et al.* 2001), which correlate strongly with the vorticity field (Rivera *et al.* 1998). For every single image, we calculated the absolute gradient field and median filtered it (MATLAB 2007; medfilt2, 5 × 5 pixels) to eliminate

Electronic supplementary material is available at http://dx.doi.org/10.1098/rsbl.2009.0806 or via http://rsbl.royalsocietypublishing.org.

One contribution of 11 to a Special feature on 'Control and dynamics of animal movement'.

Received 5 October 2009
Accepted 12 January 2010

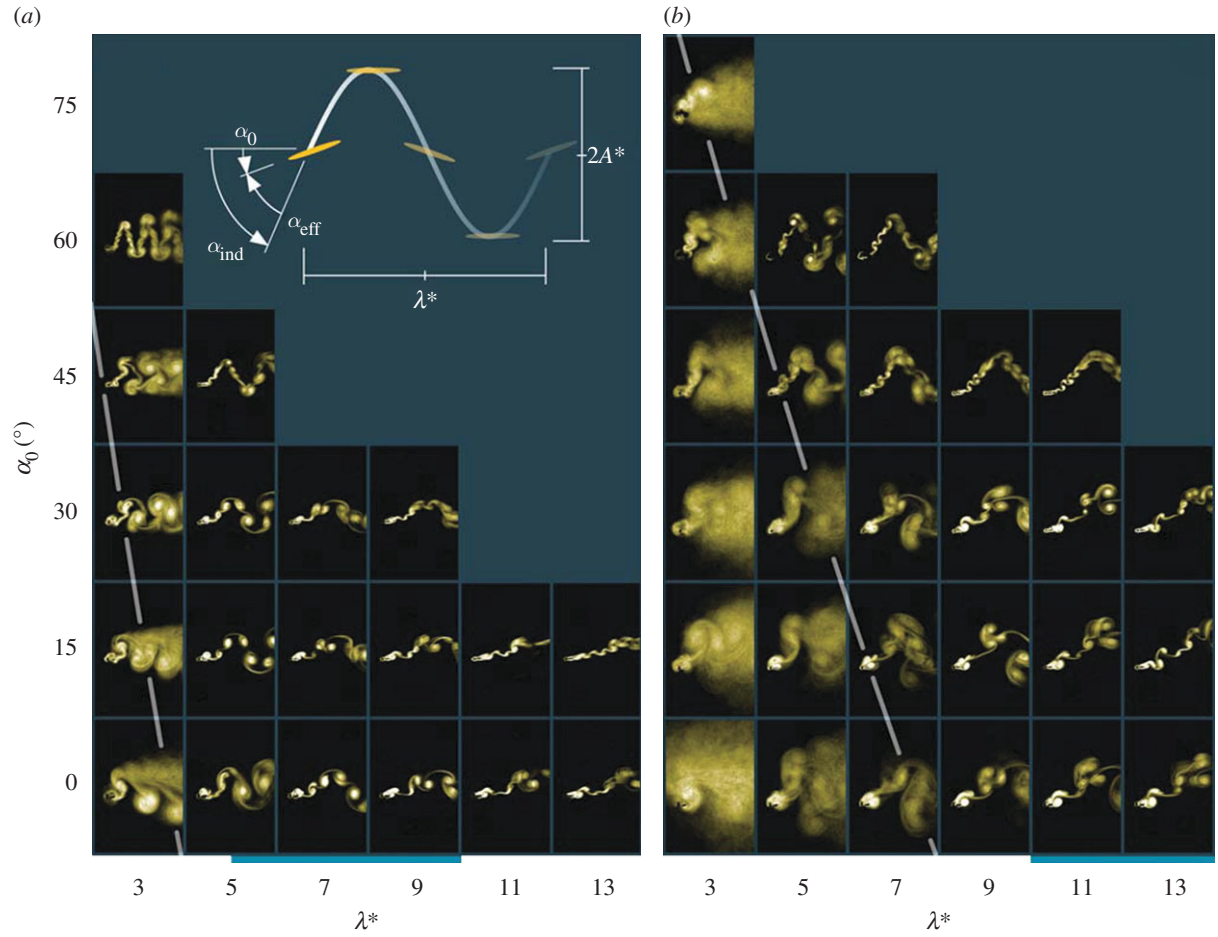

Figure 1. Phase-locked averages wake images reveal abundant chaotic vortex-wake interactions as a function of flapping foil kinematics; dimensionless heave amplitude A^* and wavelength λ^*, and pitch amplitude α_0, which are illustrated in (*a*). (*a*) $A^* = 1$; (*b*) $A^* = 2$. Empty spaces represent $\alpha_{eff} < 0^\circ$ (no thrust) for which we made no measurements. White lines (dashed) indicate the borderline between chaotic and periodic flow according to $\lambda^* = 2\pi \times A^*/\tan(50^\circ + \alpha_0/4)$ (see text for definition). The blue bar under the figure indicates the range of λ^* at which swimming and flying animals are known to cruise for the corresponding A^* (which together build up the corresponding Strouhal number range).

background fringes. Next, small pollutants were automatically removed (MATLAB; bwareaopen). After normalizing the intensity of these images, we averaged them over all 99 images for stroke reversal and midstroke. For periodic flows, this average image is identical to the individual images of the vortex wake, and therefore crisp (frame-by-frame inspection revealed no higher order harmonics, which is quantitatively supported by the electronic supplementary material, figure S2). For chaotic flow, the vortex wake varies erratically over the 99 frames and the average image is therefore blurred. We enhanced the dynamic range of all average images and coloured them using identical and automated PHOTOSHOP image adjustments (auto levels, shadow/highlight, tri-tone colouring).

(d) *Force and moment integrals*

We quantify chaos (Lorenz 1963) by calculating the standard deviation of the moment of area integrals of the 99 phase-locked image intensity fields I for stroke reversal and midstroke. This standard deviation should be close to zero for purely periodic flow. First, we create black and white images using a cut-off value of 0.17, which results in $I = 1$ where we visualized vortices and $I = 0$ elsewhere. Next, we determined the first three polar moments of area of I: $I_0 = \iint I \mathrm{d}x\mathrm{d}y$; $I_{1,r} = \left(\iint xI\mathrm{d}x\mathrm{d}y^2 + \iint yI\mathrm{d}x\mathrm{d}y^2\right)^{1/2}$; $I_{2,r} = \iint (x^2 + y^2) I\mathrm{d}x\mathrm{d}y$ for the near wake (integration area starts $c/4$ behind the foil and has width $8c$ and height $16c$). Wu (1980) shows that, if we calculate these moments using the vorticity field instead of I, I_0 would represent circulation, whereas $I_{1,r}$ and $I_{2,r}$ would be part of the integrals for calculating net force and moment, respectively. Because $I = 1$ represents the integration area where the vorticity is non-zero, we can assume that chaotic variation of I_0, $I_{1,r}$ and $I_{2,r}$ indicates that the corresponding circulation, force and moment integrals will vary chaotically too. The required fidelity for neural control depends on the short-term fluctuation. Therefore, we eliminated slow fluctuations by subtracting the period-16 Butterworth filtered time sequence (MATLAB, fourth-order Butterworth). We use the (phase-averaged) standard deviation of the short-term variation as a quantitative proxy for chaos.

3. RESULTS

The phase-locked average images of the vortex wakes reveal a boundary between a region of periodic (crisp images) and chaotic (blurred images) wakes as a function of flapping kinematics; figure 1 ($A^* = 1$, 2) and figure 2*a* ($A^* = 3$) (see the electronic supplementary material, figure S1 for $A^* = 0$, 4). Several crisp images of common periodic wake types can be found at relatively low wavelengths for $A^* = 1$, such as 'two vortex pairs' ($\lambda^* = 5$, $\alpha_0 = 15^\circ$, 30°) and 'two single vortices' ($\lambda^* = 5$, $\alpha_0 = 0^\circ$) per flap period (figure 1). Such periodic vortex configurations are both found in the wakes of fishes as a function of swimming kinematics (e.g. Müller *et al.* 2001; Borazjani & Sotiropoulos 2008). At shorter wavelengths and higher amplitudes, the wakes are chaotic resulting in blurred images of the wake, the border between periodic and chaotic vortex wakes shifts to higher wavelengths for higher amplitudes.

We find that the normalized standard deviation in I_0, $I_{1,r}$ and $I_{2,r}$ is similar valued (see the electronic

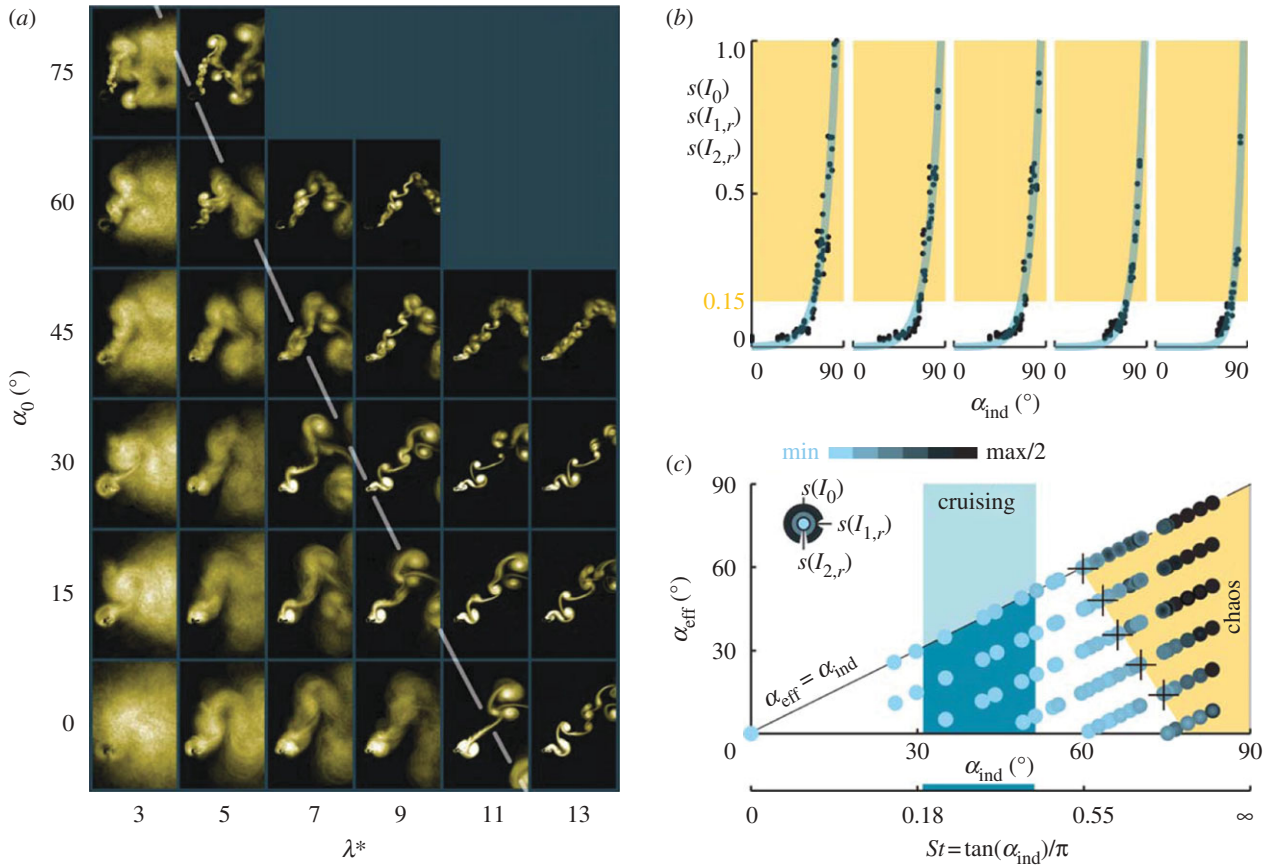

Figure 2. (*a*) Phase-locked averages wake images for $A^* = 3$ (figure 1). (*b*) Pooled normalized standard deviation of I_0, $I_{1,r}$ and $I_{2,r}$ (with respect to maximum value) as a function of α_{ind} at constant α_0 shows approximately exponential growth. Exponential fits from left to right for pooled I yield $s(I) = 1100 \times 10^{-6} e^{0.082\alpha_{ind}}$ ($\alpha_0 = 0°$; $r^2 = 0.95$); $s(I) = 700 \times 10^{-6} e^{0.084\alpha_{ind}}$ ($\alpha_0 = 15°$; $r^2 = 0.94$); $s(I) = 210 \times 10^{-6} e^{0.10\alpha_{ind}}$ ($\alpha_0 = 30°$; $r^2 = 0.92$); $s(I) = 93 \times 10^{-6} e^{0.10\alpha_{ind}}$ ($\alpha_0 = 45°$; $r^2 = 0.97$); $s(I) = 1.1 \times 10^{-6} e^{0.16\alpha_{ind}}$ ($\alpha_0 = 60°$; $r^2 = 0.91$). (*c*) Standard deviation of I_0 (outer circle), $I_{1,r}$ (middle circle), and $I_{2,r}$ (inner circle) plotted as a function of α_{eff} and α_{ind}, which are colour-coded from minimum to maximum/2; $(0.4c)^2 \leq s(I_0) \leq (2.6c)^2$; $(1.2c)^3 \leq s(I_{1,r}) \leq (4.1c)^3$; $(2.1c)^4 \leq s(I_{2,r}) \leq (5.6c)^4$. We find a periodic vortex-wake domain at low values of α_{ind} (which corresponds with Strouhal number) and a chaotic domain at high values (yellow area). The border between both domains can be described by $\alpha_{eff} = 247° - 3.15\alpha_{ind}$ and represents the left border of the yellow area (crosses indicated the calculated intersections in (*b*) to which the borderline is fitted). Animals preferably cruise at low Strouhal numbers St, in the range 0.2–0.4 (Taylor *et al.* 2003), for which we find solely periodic vortex-wake interactions.

supplementary material, figure S2 for evidence) and grow roughly exponentially as a function of α_{ind} at constant α_0, figure 2*b*. This illustrates the dramatic growth in variance in the moment of area integrals owing to chaos. We define the chaos boundary at 15 per cent of the maximum standard deviation in I_0, $I_{1,r}$ and $I_{2,r}$ in figure 2*b* and capture it through fitting the combined normalized standard deviations of I_0, $I_{1,r}$ and $I_{2,r}$ with an exponential function as a function of α_{ind} at constant α_0 (0°, 15°, 30°, 45°, 60°; we excluded 75°, because data lacked for a proper fit) and calculating the intersection.

To determine how relevant chaos could be for our understanding of animal propulsion through fluids, we plot our proxy for chaos, the standard deviations of I_0, $I_{1,r}$ and $I_{2,r}$ (§2), as a function of effective and induced angle of attack, figure 2*c*. This condensed plot for $A^* = 1–4$ features our linear approximated borderline between chaotic and periodic wakes, which we calculated as follows. We linearly fitted the intersection values of α_{ind} at 15 per cent of the maximum standard deviation in figure 2*b* and the corresponding values of α_{eff} (plotted in figure 2*c*). The linear fit $\alpha_{eff} = 247° - 3.15\alpha_{ind}$ describes the 15 per cent maximum standard deviation boundary between chaotic and periodic flows well ($r^2 = 0.99$). This boundary yields similar chaos boundaries in figures 1*a*,*b* and 2*a*: $\lambda^* = 2\pi \times A^*/\tan(50° + \alpha_0/4)$ (rounded coefficients) that match well with the transition between sharp (periodic) and blurry (chaotic) wake images.

4. DISCUSSION

Our study of vortex wakes generated by a two-dimensional flapping foil reveals that vortex wakes of flapping foils are chaotic for $\lambda^* < 2\pi \times A^*/\tan(50° + \alpha_0/4)$ and ($A^* = 1–4$; $\lambda^* = 3–13$; $\alpha_0 = 0–90°$; $Re \approx 1000 \times \sqrt{1 + (4A^*/\lambda^*)^2}$). This borderline also predicts the wavelengths for which chaos (Lentink & Gerritsma 2003) and aperiodicity (Lentink *et al.* 2008) have been reported within the range of kinematics studied here (Lewin & Haj-Hariri (2003) and Alben & Shelley (2005) studied $A^* < 1$, while Blondeaux *et al.* (2005) and Iima (2007) studied $\lambda^* < 3$).

How relevant are chaotic vortex-wake interactions for swimming and flying animals? Our study is representative for cruising flight and swimming only, because we consider $\lambda^* \geq 3$ and because two-dimensional foils approximate the flow around foils of three-dimensional wings best during forward flight (Lentink & Dickinson 2009). During cruising, animals predominantly operate at Strouhal numbers $St = \tan(\alpha_{\mathrm{ind}})/\pi$ in the range 0.2–0.4 (Taylor *et al.* 2003), which has been found to yield high propulsive efficiency (Triantafyllou *et al.* 1993). For this cruising *St*-range, we find only periodic vortex wakes; see blue region in figure 2*c* and the corresponding λ^* range indicated with a blue horizontal bar in figure 1. Our model experiments suggest that swimming and flying animals might encounter chaotic vortex-wake interactions when swimming or flying slower than $\lambda^* < 2\pi \times A^*/\tan(50^\circ + \alpha_0/4)$.

Even though our two-dimensional flapping foil model is a highly simplified representation of an animal wing or fin, which ignores three-dimensional flow and high Reynolds number effects, it seems unlikely that including these three-dimensional effects in a vortex-dynamic study of animal locomotion will suppress chaos altogether. We therefore predict that animals could tune their kinematics to evade the chaos of vortex-wake interactions. Butterflies might be interesting candidates for studying if some animals do exploit chaos—the so-called 'butterfly effect' of chaos might help make their flight paths more erratic to confound predators (Dudley 2000).

This research has been funded by NWO-ALW grant 817.02.012.

Alben, S. & Shelley, M. 2005 Coherent locomotion as an attracting state for a free flapping body. *Proc. Natl Acad. Sci.* **102**, 11 163–11 166. (doi:10.1073/pnas.0505064102)

Blondeaux, P., Guglielmini, L. & Triantafyllou, M. S. 2005 Chaotic flow generated by an oscillating foil. *AIAA J.* **43**, 918–922. (doi:10.2514/1.8042)

Borazjani, I. & Sotiropoulos, F. 2008 Numerical investigation of the hydrodynamics of carangiform swimming in the transitional and inertial flow regimes. *J. Exp. Biol.* **211**, 1541–1558. (doi:10.1242/jeb.015644)

Cerretelli, C. & Williamson, C. H. K. 2003 The physical mechanism for vortex merging. *J. Fluid Mech.* **475**, 41–77. (doi:10.1017/S0022112002002847)

Dickinson, M. H., Lehmann, F. O. & Sane, S. P. 1999 Wing rotation and the aerodynamic basis of insect flight. *Science* **284**, 1954–1960. (doi:10.1126/science.284.5422.1954)

Dudley, R. 2000 *The biomechanics of insect flight*. Princeton, NJ: Princeton University Press.

Iima, M. 2007 A two-dimensional aerodynamic model of freely flying insects. *J. Theor. Biol.* **247**, 657–671. (doi:10.1016/j.jtbi.2007.03.012)

Legras, B. & Dritschel, D. 1993 Vortex stripping and the generation of high vorticity gradients in two-dimensional flows. *Appl. Sci. Res.* **51**, 445–455. (doi:10.1007/BF01082574)

Lentink, D. & Dickinson, M. H. 2009 Biofluiddynamic scaling of flapping, spinning and translating fins and wings. *J. Exp. Biol.* **212**, 2691–2704. (doi:10.1242/jeb.022251)

Lentink, D. & Gerritsma, M. I. 2003 Influence of airfoil shape on performance in insect flight. AIAA Paper, AIAA-2003-3447. See: www.aiaa.org.

Lentink, D., Muijres, F. T., Donker-Duyvis, F. J. & Van Leeuwen, J. L. 2008 Vortex-wake interactions of a flapping foil that models animal swimming and flight. *J. Exp. Biol.* **211**, 267–273. (doi:10.1242/jeb.006155)

Lewin, G. C. & Haj-Hariri, H. 2003 Modelling thrust generation of a two-dimensional heaving airfoil in a viscous flow. *J. Fluid Mech.* **492**, 339–362. (doi:10.1017/S0022112003005743)

Liao, J. C., Beal, D. N., Lauder, G. V. & Triantafyllou, M. S. 2003 Fish exploiting vortices decrease muscle activity. *Science* **302**, 1566–1569. (doi:10.1126/science.1088295)

Lorenz, E. N. 1963 Deterministic nonperiodic flow. *J. Atmos. Sci.* **20**, 130–141. (doi:10.1175/1520-0469(1963)020<0130:DNF>2.0.CO;2)

Martin, B. & Wu, X. L. 1995 Shear flow in a two-dimensional Couette cell: a technique for measuring the viscosity of free-standing liquid films. *Rev. Sci. Instr.* **66**, 5603–5608. (doi:10.1063/1.1146027)

Muijres, F. T. & Lentink, D. 2007 Wake visualization of a heaving and pitching foil in a soap film. *Exp. Fluids* **43**, 665–673. (doi:10.1007/s00348-007-0379-y)

Müller, U. K., Smit, J., Stamhuis, E. J. & Videler, J. J. 2001 How the body contributes to the wake in undulatory fish swimming: flow fields of a swimming eel (*Anguilla anguilla*). *J. Exp. Biol.* **204**, 2751–2762.

Rivera, M., Vorobieff, P. & Ecke, R. E. 1998 Turbulence in flowing soap films: velocity, vorticity, and thickness fields. *Phys. Rev. Lett.* **81**, 1417. (doi:10.1103/PhysRevLett.81.1417)

Rutgers, M. A., Wu, X. L. & Daniel, W. B. 2001 Conducting fluid dynamics experiments with vertically falling soap films. *Rev. Sci. Instr.* **72**, 3025–3037. (doi:10.1063/1.1379956)

Taylor, G. K., Nudds, R. L. & Thomas, A. L. R. 2003 Flying and swimming animals cruise at a Strouhal number tuned for high power efficiency. *Nature* **425**, 707–711. (doi:10.1038/nature02000)

Triantafyllou, G. S., Triantafyllou, M. S. & Grosenbaugh, M. A. 1993 Optimal thrust development in oscillating foils with application to fish propulsion. *J. Fluid Struct.* **7**, 205–224. (doi:10.1006/jfls.1993.1012)

Wu, J. C. 1980 Theory for aerodynamic force and moment in viscous flow. *AIAA J.* **19**, 432–441. (doi:10.2514/3.50966)